

Title	Structural analysis of a roof extracted from a wind turbine blade
Authors	Gentry, T. Russell;Al-Haddad, Tristan;Bank, Lawrence C.;Arias, Franco R.;Nagle, Angela;Leahy, Paul G.
Publication date	2020-12
Original Citation	Gentry, T. R., Al-Haddad, T., Bank, L. C., Arias, F. R., Nagle, A. and Leahy, P. (2020) 'Structural Analysis of a Roof Extracted from a Wind Turbine Blade', Journal of Architectural Engineering, 26(4), 04020040. doi: 10.1061/(ASCE)AE.1943-5568.0000440
Type of publication	Article (peer-reviewed)
Link to publisher's version	<a href="https://ascelibrary.org/doi/pdf/10.1061/%28ASCE%29AE.1943-5568.0000440">https://ascelibrary.org/doi/pdf/10.1061/%28ASCE%29AE.1943-5568.0000440</a> - 10.1061/(ASCE)AE.1943-5568.0000440
Rights	© 2020, American Society of Civil Engineers. This material may be downloaded for personal use only. Any other use requires prior permission of the American Society of Civil Engineers. The published article may be found at <a href="https://ascelibrary.org/doi/pdf/10.1061/%28ASCE%29AE.1943-5568.0000440">https://ascelibrary.org/doi/pdf/10.1061/%28ASCE%29AE.1943-5568.0000440</a>
Download date	2024-09-17 08:13:31
Item downloaded from	<a href="https://hdl.handle.net/10468/11171">https://hdl.handle.net/10468/11171</a>



# UCC

**University College Cork, Ireland**  
Coláiste na hOllscoile Corcaigh



17 (LRFD) method familiar to civil engineers. Analysis of stresses and deflections was conducted  
18 using hand calculations and the finite element method (FEM). The results of the analyses show  
19 that the roof is within code mandated stress and deflection limits. The methodology developed  
20 can be applied to other wind blade repurposing concepts.

21

22 Keywords: Recycling, Repurposing, Design, Finite element analysis, Wind turbine blades,

23

## 24 **Introduction**

25

26 Fiber Reinforced Polymer (FRP) composite materials are not biodegradable and present unique  
27 problems for waste management and their End-of-Life (EOL). The impact of polymers on the  
28 environment and society has become a major concern in many countries. In response to the  
29 European Waste Directive (DIRECTIVE 2008/98/EC, 2008), the option of disposing of end-of-  
30 life FRP blades in landfills is now restricted by landfill taxes and reuse, recycling and recovery  
31 targets. Since the 1990s, there has been a developing body of research that has studied the issues  
32 of recycling and EOL of FRP composites, in general, and composite wind blades, in particular.  
33 Recent analyses of the key issues related to the EOL of wind turbine blades can be found in Liu  
34 and Barlow (2017), Jensen and Skelton (2018) and Bank et al. (2018). For example, a typical 2.0  
35 MW turbine with three 50 m blades has approximately 20 tonnes of FRP material and an 8 MW  
36 turbine has approximately 80 tonnes of FRP material (based on a conservative 1 MW  $\approx$  10  
37 tonnes of FRP conversion). Based on a predicted “moderate growth scenario” from the Global  
38 Wind Energy Council (GWEC), waste blades from future wind power installations will total of  
39 16.8 million tonnes by 2030 and 39.8 million tonnes by 2050 if no action is taken in the interim

40 (GWEC, 2016). At the present time numerous large (40 to 60 meter) composite material wind  
41 turbine blades are coming out of service due to their original 20-year design life or due to  
42 replacement by more efficient turbines and/or blades (referred to as repowering).

43

#### 44 **Managing Composite Material “Waste”**

45

46 There are various methods to manage waste composites (either production waste or EOL waste  
47 products) at the present time (Oliveux et al., 2015, Job et al, 2016) – some of which are referred  
48 to as “recycling”. Unfortunately, the term “recycling” has many different meanings in this field  
49 and the term “second-life” is preferred so there is a clear understanding of their position in a  
50 waste processing hierarchy. Following Skelton (2017) and Jensen and Skelton (2018) we  
51 propose the following categorization of second-life options for FRP wind blades;

52

53 1. **Reuse:** In this scenario the entire blade is reused. The blade is used as a turbine blade in its  
54 second life but has its lifetime extended by refurbishment or remanufacturing or is sold on  
55 the second-hand market.

56 2. **Repurpose:** In this scenario the structural properties and the material properties of the  
57 composite are repurposed. The blade is used whole or sectioned into parts and repurposed for  
58 other products such as parts of temporary or inexpensive housing, office and home furniture,  
59 benches and playgrounds, pedestrian bridges and powerline structures (Bank et al., 2018;  
60 Adamcio, 2019; Bladesign, 2019, SuperuseStudios, 2012; Speksnijder, 2018; Suhail et al.,  
61 2019; Anmet, 2019; Bank et al, 2019; Alshannaq et al, 2019).

62 3. **Recycle**

63 a. **Fully-Recycle:** In this scenario the material properties of the composite are recycled.

64 The blade is cut, shred or ground into small pieces or granular material as filler for  
65 use in concrete or other composites (Beauson et al, 2016; Mamanpush et al, 2018;  
66 Yazdanbakhsh et al, 2018; Rodin et al., 2018).

67 b. **Partially-Recycle:** In this scenario the glass fiber constituent of the composite is  
68 used. This includes thermo–chemical methods such as pyrolysis, solvolysis,  
69 thermolysis (fluidized bed) (Oliveux et al 2015) that are used to reclaim the glass  
70 fiber. Or the glass fiber is used as a feedstock for cement clinker by co-processing the  
71 shredded composite material in a cement kiln (Ramesh et al 2018).

72

73 Waste disposal methods such as landfilling or incineration, with or without energy recovery, or  
74 syngas production are not considered to be second-life methods since no material is reused in a  
75 new product. Clearly, all the second-life methods listed above will need “third-life” or other  
76 disposal methods in the future. In most of the world landfilling is the predominant method of  
77 disposing of FRP scrap and EOL waste costing in the range of \$45 to \$200 per ton. With the  
78 increased awareness of the environmental impacts of climate change, decreased and more  
79 expensive natural resources, and greater global concerns for health, the barriers to FRP  
80 production and waste disposal are likely to increase.

81

82 In what follows the repurposing of a part extracted from a 100 m long FRP blade as a roof  
83 structure is discussed. Fig. 1 shows conceptual designs for platform foundations, doors and  
84 window shutters, roof panels and roof for small (approx. 40 m<sup>2</sup>) masonry block houses (Bank et  
85 al, 2018.) Such buildings are ubiquitous in the developing world. Of the different possible uses

86 of the blade parts shown in Fig. 1, the roof was chosen for further detailed structural analysis  
87 because of its large size and complex geometry and materials. The study follows and expands a  
88 prior conceptual study of a similar roof structure with different geometry and calculations (Bank  
89 et al, 2019.)

90

## 91 **Wind Blade Geometry**

92

93 The wind blade selected for the current work was a 100 m long prototype wind blade designed  
94 by Sandia National Laboratories (SNL) identified as SNL-100-01 (Griffith, 2013). This blade is  
95 similar in size to a 107-meter turbine blades currently being manufactured for a 12 MW turbine  
96 (General Electric, 2019). The geometry is defined by 25 different airfoils at specific stations  
97 along the blade length from the root end, where the blade is connected to the turbine hub, to the  
98 tip. The materials are defined by 393 different solid and sandwich composite material lay-ups.  
99 The SNL-100-01 model of the blade is a two-dimensional wire frame (surface) model built using  
100 the Numerical Manufacturing and Design Tool (NuMAD) (Berg and Resor, 2012, Arias, 2016).  
101 A three-dimensional architectural model of the blade including thickness and material types at all  
102 locations is required for architectural and structural calculations and detailing. Fig. 2. shows the  
103 three-dimensional model of the 100-meter blade which was built from the stack layups and  
104 material types provided in Griffith (2013) using Rhino 3D (Rhino, 2017, Arias, 2017)

105

106 The blade has a maximum chord (i.e., the distance between the leading edge and trailing edge) of  
107 7.628 m at a distance of 19.5 m from the root end. The blade has a foam core shell, three internal  
108 foam core webs (identified as SW1, SW2 and SW3 from left to right in Fig. 2(b)) and a carbon

109 fiber spar cap (shown in black above and below the webs SW1 and SW2). The part of the 100  
110 meter blade that was extracted from the three-dimensional blade model to create the roof region  
111 was extracted from Station 19 to Station 20 (27.6 m to 35.8 m) and is shown schematically in  
112 Fig. 3.

113

114 A schematic rendering of the part used for the roof is shown on the masonry block walls of the  
115 approximately 40 m<sup>2</sup> house in Fig. 4. Fig. 4 also shows schematics of the connection details  
116 using Simpson Strong-Tie<sup>®</sup> straps between the blade roof and the masonry walls. Fig.4 also  
117 shows schematics of louvre type window shades to enclose the open ends of the blade roof.  
118 Louvre type windows and shades are commonly used in informal housing in developing  
119 countries where high humidity and temperatures are common (Bank et al 2018)

120

## 121 **Structural Analysis of the Roof**

122

### 123 Dimensions

124

125 The center-line dimensions of the roof used in the calculations that follow are shown in Fig. 5.

126

### 127 Materials

128 The mechanical and physical properties of the materials as well as their layups in different  
129 locations around the cross-section and along the length of the SNL-100-01 blade are given in  
130 Griffith (2013). These are based on the MSU material test database (Mandell et al 1997, SNL

131 2019). In cases where properties were not provided in Griffith (2013) they were obtained from  
132 the literature as noted in Table 1.

133

134 The geometric and material properties of the roof were determined for the laminates and  
135 sandwich panels for the region from Station 19 to Station 20 (27.6 m to 35.8 m). These were  
136 used in both hand calculations and in the LS-DYNA finite element method (FEM) analysis in  
137 what follows. The as-reported properties given in Griffith were used in the analysis. Any changes  
138 in material properties or dimensions due to the expected 20-year in-service operation of the blade  
139 were not considered at this time. The estimation of residual properties in wind blades after 20  
140 years of service (known as remaining-life) is an active research field (Post et al 2008).

141

#### 142 Design Philosophy

143

144 For civil engineering structural analysis of composite material structures the Load and Resistance  
145 Factor Design (LRFD) (or its equivalent called Limit States Design (LSD) in the EU) methods or  
146 Allowable Stress Design (ASD) methods are used (Bank, 2006). The two primary limits states  
147 analyzed are the Ultimate Limit State (ULS) and the Serviceability Limit State (SLS). In the  
148 ultimate limit state (strength, stability) analysis, nominal service loads are typically increased  
149 using prescribed load factors and the structural or material capacities are typically reduced using  
150 prescribed resistance or materials safety factors. In the serviceability limit state (deflections,  
151 vibrations etc.), neither the nominal service loads nor the material properties are typically  
152 factored. The loads for the ULS and SLS are referred to as the factored loads or the service loads,  
153 respectively.



154

155 Nominal service live loads and load combinations (load cases) are used for a civil engineering  
156 structural design and are stipulated in ASCE 7-16 (2016) or Eurocode EN 1991: Actions on  
157 structures (1991). Load combinations are factored amounts of nominal dead load, live load, roof  
158 live load, wind load, snow load, and others (ASCE 7-16).

159

160 The resistance or material factors depend on the type of materials used and are given in separate  
161 material specific design codes (e.g., for concrete, the ACI 318-19 or EN 1992: Design of  
162 concrete structures; CEN 1992) At the time of writing (2019) an approved design code does not  
163 exist for composite materials for civil engineering structures. An ASCE Standard and a Eurocode  
164 are currently under development. In the absence of a code the material factors for the FRP  
165 materials used in this analysis are taken from EUR (2016), the precursor document to the  
166 Eurocode. The Material Partial Factor,  $\gamma_M$ , for ultimate strength was calculated to be  $\gamma_M = (1.15$   
167  $\times 1.35 \times 1.2) = 1.86$ , assuming (1) the material properties were obtained by test ( $\gamma_{M1} = 1.15$ ), (2)  
168 the production processes and properties of the materials have a standard deviation  $\leq 0.10$  ( $\gamma_{M2} =$   
169  $1.35$ ), and, (3) be the material was not post-cured ( $\gamma_{M3} = 1.2$ ).

170

171 For the serviceability analysis the nominal service loads are used and the Material Partial Factor,  
172  $\gamma_M = 1.0$ . For most structures the serviceability requirements are set by building codes (e.g.,  
173 International Building Code (IBC 2018)). For roof structures the requirement is typically that the  
174 deflection,  $\delta$ , (displacement downwards due to gravity) be  $\delta < L/240$  (i.e., the member span  
175 divided by 240)

176

177 It is also of interest to note that design codes for composite wind blades themselves are not yet  
178 available. Technical Committee TC 88, working group PT 61400-5 of the International  
179 Electrotechnical Commission (IEC) is currently working on IEC 61400 - Part 5: Rotor blades.  
180 However, even when these codes are published, they will not be suitable for structural design for  
181 civil structures since local authorities provide construction permits for projects based on building  
182 codes such as the International Building Code (ICC, 2018) which incorporate the model material  
183 design codes (e.g., ACI-318).

184

#### 185 Loads for roof design

186

187 For the purposes of the proof-of-principle analysis presented in this paper only one load  
188 combination was considered: Dead Load + Roof Live Load ( $D + L_r$ ). Only a uniform dead load  
189 was considered. Concentrated live load, wind, snow or ice load on the roof load were not  
190 considered at this time. This was done to demonstrate the methodology needed for such  
191 calculations. It is important to note that other load cases especially those related to wind loads  
192 also need to be analyzed. Wind load can create uplift on a roof system which could affect not  
193 only the design of the roof itself but, perhaps more significantly, the design of the connection  
194 details and louvres shown in Fig. 4.

195

196 The dead load was determined by uniformly distributing the entire 24.32 kN weight of the roof  
197 (determined from the material densities and volumes) over the entire projected roof area of 42.9  
198  $m^2$ . This gave a uniformly distributed dead load,  $D = 0.566 \text{ kN/m}^2$ . The code stipulated roof live

199 load,  $L_r = 0.96 \text{ kN/m}^2$  was used. This gives an unfactored service load of  $1.52 \text{ kN/m}^2$  and a  
200 factored load of  $1.2(0.566) + 1.6(0.96) = 2.212 \text{ kN/m}^2$  (ASCE 7-16 LRFD load combination 3).

201

## 202 **Preliminary Analysis - Hand calculations**

203

204 Hand calculations using one-dimensional mechanics of materials models were used to determine  
205 stresses in individual elements of the roof – Case (1) the shell panel between the 2<sup>nd</sup> shear web  
206 and the trailing edge, and Case (2) the third shear web of the roof section. These two cases were  
207 chosen for the hand calculations since they were found to be those that gave the largest local  
208 deflections and stresses in the roof structure based on a prior approximate analysis conducted  
209 (Bank et al 2019). Simplifying assumptions were made relative to the boundary conditions of the  
210 shell and web sandwich panels in order to obtain a rough order of magnitude (ROM) estimate of  
211 the stresses prior to conducting the detailed FEM analysis described in the following section.  
212 Such analyses are routinely made in the early conceptual design stages by structural engineers  
213 and architects.

214

### 215 (1) Out-of-Plane Bending of the Shell Panel

216

217 The sandwich panel at the chosen location in the blade consists of a 60 mm thick thermoplastic  
218 foam core and two 5 mm composite material face skins of SNLTriax (see Table 1). Since this  
219 shell panel is in the transverse (contour) orientation relative to the blade (and roof) longitudinal  
220 axis the transverse stiffness and strength properties of the materials are used:  $E_{22(\text{Triax})} = 13.65$

221 GPa,  $E_{\text{foam}}=0.256$  GPa,  $\sigma_{22(\text{Triax})} = +144$  MPa,  $\sigma_{22(\text{Triax})} = -213$  MPa,  $\sigma_{\text{tens(foam)}} = +3.1$  MPa,  
 222  $\sigma_{\text{comp(foam)}} = -3.8$  MPa, and  $\tau_{\text{ult(foam)}} = 2.0$  MPa (see Table 1).

223

224 The shear web sandwich panels consist of a 60 mm thick thermoplastic foam core and two 3 mm  
 225 composite material face skins of SNLBiax (see Table 1). Since the shear web sandwich panels  
 226 are parallel to the blade (and roof) longitudinal axis the longitudinal stiffness and strength  
 227 properties of the materials are used:  $E_{11(\text{biax})} = 13.60$  GPa,  $E_{\text{foam}}=0.256$  GPa,  $\sigma_{11(\text{Biax})} = +144$  MPa  
 228 and  $\sigma_{11(\text{Biax})} = -213$  MPa.

229

230 The critical shell panel for analysis was assumed to span between the second web and the trailing  
 231 edge over the third web as shown in Fig 6. It was analyzed as a flat continuous beam of unit  
 232 width (1 m) over three supports: S1 second web (0.9 m); S2 third web (0.6m); and S3 the trailing  
 233 edge. The end supports at the trailing edge and the second web (0.90 m deep) were assumed to  
 234 be pinned while the middle support (0.60 m web) was assumed to be an elastic spring support  
 235 with a stiffness equal to the in-plane stiffness of the web. The spans were 1.81 m and 1.94 m  
 236 respectively.

237

238 Using the transformed section method the SNLtriax skins were transformed into the properties of  
 239 the core ( $n_1 = 13.65/0.256 = 53.3$ ) to give a transformed second moment of the 70 mm thick shell  
 240 panel of  $I_{t(\text{shell})} = 5.82 \times 10^8$  mm<sup>4</sup>. For the 600 mm deep shear web 3 the SNLBiax skins were  
 241 transformed to the properties of the core ( $n_2 = 13.60/0.256 = 53.1$ ) to give a transformed second  
 242 moment of the 600 mm deep web of  $I_{t(\text{web})} = 6.84 \times 10^9$  mm<sup>4</sup>. The flexural stiffness of the shell  
 243 is calculated as,  $E_c I_{t(\text{shell})} = 1.49 \times 10^{11}$  N.mm<sup>2</sup> and that of the web  $E_c I_{t(\text{web})} = 1.75 \times 10^{12}$  N.mm<sup>2</sup>.

244 Solving the indeterminate structure in Fig. 6 for the contact force,  $R_2$ , between the shell and the  
 245 web gives the support reactions due to factored loads,  $R_1 = R_3 = 2694$  N,  $R_2 = 2876$  N. The  
 246 maximum moment occurs at  $x = 1223$  mm from S1 and is equal to  $M_{\max} = 1.64 \times 10^8$  N-mm.  
 247 The maximum shear force is  $V_{\max} = 2694$  N. The maximum tensile and compressive stresses in  
 248 the top shell skin is  $\sigma_{\text{Triax\_skin}} = \pm 5.26$  MPa and the core of  $\sigma_{\text{foam}} = \pm 0.085$  MPa. The shear stress  
 249 in the core is  $\tau_{\text{foam}} = 2694 / (60)(1000) = 0.045$  MPa. The downward deflection of shell due to  
 250 service loads at  $R_2$  was  $\delta = 12.08$  mm.

251

## 252 (2) In-plane Bending of the Shear Web

253

254 The 600 mm deep by 8000 mm long web is loaded by a tributary area of half the distance (1.81  
 255 m) to SW2 on the left side and half the distance (1.94 m) to the trailing edge on the right side as  
 256 shown in Fig. 7. The web is assumed to be simply-supported at its two ends (spanning between  
 257 the short-end walls of the house) and connected to the shell at its top edge. It is analyzed as a T-  
 258 beam. The effective width of the T-beam flange is taken as  $b_{\text{eff}} = b_{\text{web}} + 16(t_{\text{shell}}) = 66 + 16(70) =$   
 259  $1186$  mm which is less than  $L/4 = 2000$  mm or the web spacing,  $S = 1810$  mm (ACI 318-19).  
 260 For this configuration the SNLTriax skin is in its longitudinal direction and the longitudinal  
 261 stiffnesses and strength properties are used:  $E_{11(\text{Triax})} = 27.7$  GPa,  $\sigma_{11\text{tens}(\text{Triax})} = +972$  MPa,  
 262  $\sigma_{11\text{comp}(\text{Triax})} = -702$  MPa. Properties of the shear web and the foam are as in Case (1) above.

263

264 Using the transformed section method the SNLTriax and SNLTriax skins were transformed into  
 265 the properties of the core ( $n_1 = 27.7/0.256 = 108.2$ ,  $n_2 = 13.60/0.256 = 53.1$ ) above giving  $\bar{Y} =$   
 266  $589$  mm from the bottom of the web and  $I_t = 2.90 \times 10^{10}$  mm<sup>4</sup>. The uniform line load (factored)

267 on the top of the web was calculated to be 4.16 N/mm. The maximum bending moment at  
 268 midspan assuming simple supports at the 8-m ends was  $M_{\max} = 3.31 \times 10^7$  N-mm and the  
 269 maximum shear force at the supports was  $V_{\max} = 16,640$  N. The maximum positive and negative  
 270 flexural stresses at midspan were  $\sigma_{\text{Triax\_top}} = -10.06$  MPa,  $\sigma_{\text{Biax\_bot}} = +36.06$  MPa,  $\sigma_{\text{foam\_shell}} = -$   
 271  $0.087$  MPa,  $\sigma_{\text{foam\_web}} = -0.680$  MPa,  $\tau_{\text{foam\_web}} = 0.462$  MPa (assuming the web foam core carries  
 272 all the shear force). The maximum displacement (deflection) under service loads at midspan was  
 273 29.9 mm. (span/268).

274  
 275 If the T-beam web is assumed to be fixed-fixed at its ends the maximum deflection is 5.98 mm  
 276 (span/1338) and the maximum stresses at midspan (positive moment) are: In the panel Triax skin  
 277  $\sigma_{\text{Triax\_top}} = -3.35$  MPa and in the web Biax skin  $\sigma_{\text{Biax\_bot}} = +12.01$  MPa, and the maximum stresses  
 278 at the fixed support (negative moment) in the panel Triax skin  $\sigma_{\text{Triax\_top}} = +6.71$  MPa and in the  
 279 web Biax skins  $\sigma_{\text{Biax\_bot}} = -24.02$  MPa (all four stresses need to be determined since the section is  
 280 unsymmetric and both positive and negative moment regions exist.)

281  
 282 Overdesign Factor – Hand Calculations

283  
 284 Comparing the calculated stresses and displacements to the material strengths and the code  
 285 specified deflection limits (L/240 in this case) indicates the amount of overdesign. It is important  
 286 to note that this not the safety factor which is accounted for in the load and material factors used.  
 287 Ideally the structural designer attempts to get the overdesign factor (ODF) as close as possible to  
 288 1.0. In the current repurposing design the structure and its properties are predetermined by the  
 289 original design (as a wind blade) and the stresses and deflections are checked with allowable

290 values. The properties of the section cannot be changed as in a typical design iteration (although  
291 they can be modified with local stiffeners and strengtheners). The architectural design is  
292 performed at the conceptual stage where the repurposing concept is developed for different sizes  
293 of blades. Hence the structural analysis is done to verify the acceptability of stresses, deflections  
294 and overdesign factors as opposed to the safety factors that need to be reported. The level of  
295 overdesign for the two cases considered above is presented separately for purposes of discussion  
296 but, in reality, the lowest number obtained is the actual overdesign factor for the entire structure.  
297

298 The calculated stresses and displacements and their relevant allowable values and overdesign  
299 factors for Case 1 are shown in Table 2. The critical stress for the shell panel is the tensile stress  
300 in the transverse direction SNLTriax material in the top layer; but the ODF = 14.7 is high which  
301 indicates low utilization of the material capacity. However, the deflection is closer to the code  
302 requirement with an ODF = 1.29. Since all overdesign factors are  $> 1.0$  the shell panel has  
303 sufficient strength and stiffness under this loading condition. For large glass fiber composite  
304 material structures, it is common that serviceability conditions control the design (Bank, 2006).  
305

306 The calculated stresses and displacements and their relevant allowable values and overdesign  
307 factors for Case 2 are shown in Table 3. The critical stress for the shell panel is the tensile stress  
308 in the longitudinal direction of the SNLBiAx material in the web skins, with an ODF = 2.1. The  
309 foam core critical shear stress in the web has an ODF = 2.4. Again, the serviceability condition  
310 controls the design with an ODF = 1.1. Nevertheless, all ODFs are  $> 1.0$  for these hand-  
311 calculations and the structure is safe and serviceable. Note that the results shown in Table 3 for  
312 the shear web are for the less conservative analysis that assumes that the shear web is pin-roller

313 supported (as opposed to fixed-fixed) at its ends. ODFs will be higher if the fixed-fixed  
314 conditions are used.

315

### 316 **Detailed analysis – finite element method**

317

318 The finite element modeling of the roof was conducted using the implicit version of the LS-  
319 DYNA software code (LS-DYNA, 2018). LS-DYNA implicit was chosen because the authors  
320 have detailed knowledge and many years of experience working with this code (both the implicit  
321 and explicit forms (e.g., Bank and Gentry (2001)). Unfortunately, finite-element codes of this  
322 type are not ideally suited to structural engineering analysis since they do not allow “automatic”  
323 evaluations of standard ASCE 7 load cases. This means that the load cases must be input  
324 manually which is not trivial. Equally unfortunate is that standard structural engineering design  
325 codes (e.g., ETABS, STAAD, ROBOT) do not permit arbitrary laminated composite plate and  
326 shell elements.

327

328 The FEM mesh, global ( $X, Y, Z$ ) and local ( $x, y, z$ ) coordinate systems for the shell and the webs,  
329 and the boundary conditions are shown in Fig. 8. In Fig. 8 triangles represent pinned supports  
330 and circles roller supports and grey circles indicate support hidden from view in this orientation.  
331 The colors in the model represent different layups in segments of the blade that were used in the  
332 roof. The foreshortened perspective shown in Fig. 8 is drawn looking from the 35.8 m station  
333 towards the 27.6 m station (i.e., tip to root of the blade).

334



335 The yellow region is the Carbon Fiber Reinforced Polymer (CFRP) / Glass Fiber Reinforced  
 336 Polymer (GFRP) spar cap between webs 1 and 2 (5 mm SNLTriax/80 mm SNLCarbon/5 mm  
 337 SNLTriax), the green regions are the GFRP/foam shell sandwich panel (5 mm SNLTriax/60 mm  
 338 foam/5 mm SNLTriax), the brown region is the trailing edge panel (TE) (5 mm SNLTriax/15  
 339 mm Glass UD/40 mm Foam/5 mm SNLTriax), and the blue regions are the SNLBiax/foam web  
 340 panels (3 mm SNLBiax/50 mm foam/3 mm SNLBiax) (Griffith, 2013). A fully-integrated  
 341 laminated shell element (LSDYNA ELFORM=16) was used. The total model consisted of 3115  
 342 nodes and 1813 elements. The major 11-axis of the materials (see Table 1) is aligned with the  
 343 global Y-direction and the local  $x$ -direction for the shell and web segments (see Fig. 8).

344

#### 345 Results of Finite Element Analysis

346

347 Selected results from the finite element analyses are presented to illustrate the stress distributions  
 348 and displacements in key locations. As in the hand calculations the factored load in the global Z-  
 349 direction was  $2.212 \text{ kN/m}^2$ . This was uniformly distributed over the 3115 nodes in the model.  
 350 Fig. 9 shows the vertical displacement (deflection) of the roof in the negative Z-direction. The  
 351 maximum displacement of 7.1 mm (downwards) occurs over the 3<sup>rd</sup> shear web near the center of  
 352 the large panel between the trailing edge support and the 2<sup>nd</sup> shear web.

353

354 The stress at the midplane of the top surface in the SNLTriax layer in the skin of the shell  
 355 sandwich panel in the local  $y$ -direction is shown in Fig. 10. To help with visualization the shear  
 356 webs are only shown in outline in these contour plots. The maximum compressive stress in the  
 357 transverse direction of -5.0 MPa occurs in the two panels on either side of the 3<sup>rd</sup> shear web. It

358 be can be seen that the 3<sup>rd</sup> shear web provides a flexible intermediate support and the  
 359 compressive stress decreases along this line giving the butterfly shaped stress contours. The light  
 360 blue shading over the 2<sup>nd</sup> shear web indicates a tensile stress and a negative curvature (and  
 361 moment) over the support. Regions of high tensile stress in the shell top skin are also seen at the  
 362 upper ends of the 3<sup>rd</sup> shear web indicating negative curvature at the end of the flexible  
 363 intermediate support and some fixity at the ends provided by shell action.

364

365 The stress at the midplane of the top surface in the SNLTriax layer in the skin of the shell  
 366 sandwich panel in the local  $x$ -direction is shown in Fig. 11. (In this figure the stress along the  
 367 blade axis is shown,  $\sigma_x$ , while in Fig. 10 the stress transverse to the blade axis is shown,  $\sigma_y$ . Due  
 368 to two-way bending of the panel these stresses are different.) As with the  $y$ -direction the central  
 369 portion is in compression (green) with a maximum longitudinal compressive stress in this region  
 370 of -5.0 MPa. Similar to the  $y$ -direction tensile stresses are seen in the  $x$ -direction at the ends of  
 371 the 3<sup>rd</sup> shear web indicating a negative curvature in this direction as well. However, this is not as  
 372 significant as in the  $x$ -direction due to the higher stiffness of the shell skin laminate in the  $x$ -  
 373 direction.

374

375 The displacements and stress in the shear webs are shown next. To help with visualization the  
 376 shell panels are only shown in outline in these contour plots. Downwards displacement of the  
 377 shear webs is shown in Fig. 12. The maximum deflection in the  $Z$ -direction is 7.1 mm  
 378 (downwards) and occurs under the 3<sup>rd</sup> shear web which is equal to the deflection of the top shell  
 379 at this location shown in Fig. 9. This to be expected as the in-plane deformation of the shear

380 webs in the Z-direction is negligible. The maximum displacement under the 2<sup>nd</sup> shear web is  
381 significantly less and is 2.4 mm at its center. This explains the restraint provided by the 2<sup>nd</sup> shear  
382 web and the negative curvature over the webs seen in Fig. 10. The 1<sup>st</sup> shear web which is fully  
383 supported at its bottom along the wall shows no downward displacement, as expected.

384  
385 The stresses in the x-direction in the shear webs are shown in Fig.13. The maximum tensile  
386 stress occurs in the SNLBiAx skin in the 3<sup>rd</sup> shear web at the bottom of the web and is equal to  
387 10.9 MPa. Tensile stresses at the bottom of the 2<sup>nd</sup> shear web are less, with a maximum at the  
388 center of 5.7 MPa. It is interesting to note the relatively large compressive stresses of -25.0 MPa  
389 at the pinned supports of the shear webs. This implies a localized outward thrust due to a global  
390 restraint provided by the shell. It is important to note the shear webs are supported by roller  
391 supports (no restraint in the longitudinal X-direction) at their far ends (see Fig. 8) so ideally there  
392 should be no thrust at the pinned supports at the near ends. However, the shear webs do not  
393 behave as simple beams and are restrained at their ends by the global two-way action of the shell.

394  
395 The stresses in the local y-direction of the shear webs are shown in Fig. 14. Compressive  
396 stresses are noted at the supports which are larger at the near ends due to the pinned support as  
397 noted previously.

398  
399 Finally, elastic buckling analysis was conducted to check for overall instability of the roof  
400 structure. The buckling occurs at a load magnification factor of 31 (i.e., 31 times the factored  
401 load of 2.212 kN/m<sup>2</sup>.) Buckling occurs in the 3<sup>rd</sup> shear web as is shown in Fig. 15. This is logical  
402 given the large compressive stresses seen in this location in both the local x and y directions.

403 However, the buckling load is much larger than would be required to cause material failure in  
404 these locations and elastic instability will be precluded. Nevertheless, local stiffening will be  
405 needed at the supports of the 2<sup>nd</sup> and 3<sup>rd</sup> webs to prevent both local bearing failure and local  
406 buckling at these locations (Borowicz and Bank 2013).

407

#### 408 Overdesign Factor – 3-D FEM Calculations

409

410 The finite element analysis gives results for the entire structure unlike the hand-calculations  
411 where the shell and web were analyzed separately. The results for the 3-D FEM calculations are  
412 given in Table 4.

413

414 The critical stress for the roof as a whole is the compressive stress in the longitudinal direction in  
415 the SNLBiax layer in the shear web with an ODF = 4.6. All ODFs are all greater than 1.0 for  
416 this FEM analysis and the structure is safe. The critical displacement is in the shell panel with an  
417 ODF of 2.2 which satisfies serviceability requirements.

418

#### 419 **Discussion**

420

421 The results obtained from the one-dimensional mechanics-of-materials hand calculations and the  
422 full three-dimensional finite element method analyses are in reasonably good agreement.

423 Generally, the stresses and deflections obtained from the FEM analysis are less than those

424 obtained in the hand-calculations. This is to be expected as the roof shell has a two-way action

425 that distributes loads in both the transverse and longitudinal directions. It is encouraging to know

426 that provided good modeling assumptions are made for hand-calculations, these calculations can  
427 be used in preliminary design stages to assess the feasibility of repurposing designs. In addition,  
428 the FEM analysis uncovers local multi-directional stresses, especially at the supports, which  
429 provides important input for structural detailing such as local stiffening and strengthening.

430

## 431 **Conclusions**

432

433 A methodology for structural analysis of EOL wind turbine blade sections has been developed  
434 and demonstrated. This is essential for repurposing wind turbine blades. The methodology can be  
435 applied to other structural applications for decommissioned wind turbine blades. This will  
436 contribute to improved sustainability of the wind energy sector. As indicated in the paper both  
437 hand-calculations and finite element methods can be used for analysis. Nevertheless, this is not  
438 trivial as a wind blade tapers and twists and its material properties change along its length. In  
439 either case the analysis results will only be as good as the assumptions made in building the  
440 analytical models. Over-simplification of hand-calculation models is not advised. When FEM  
441 analysis is used laminated shell elements must be used and care must be taken to correctly orient  
442 the orthotropic materials in the laminate with respect to the global coordinate system.

443

444 For structural analysis and architectural detailing a full 3-D model showing the individual  
445 material layers of the blade is needed. However, most blade models used for aerodynamic and  
446 structural analysis are wire frame surface models. In addition, for infrastructure applications  
447 governing building codes will need to be used since local jurisdictions permit construction based  
448 on these codes. These codes are not typically familiar to composite material designers. At the

449 current time a code does not exist to obtain probabilistically based material partial factors or  
450 element resistance factors for design of FRP structures. But, code like documents can be and are  
451 used in lieu of these codes.

452

### 453 **Acknowledgement**

454

455 Support for this research was provided by the U.S. National Science Foundation (NSF) under  
456 grants 1701413, and 1701694; by InvestNI/Department for the Economy (DfE) under grant  
457 16/US/3334 and by Science Foundation Ireland (SFI) under grant USI-116 (US-Ireland Tripartite  
458 program).

459

### 460 **Data Availability Statement**

461

462 Some or all data, models, or code that support the findings of this study are available from the  
463 corresponding author upon reasonable request.

464

### 465 **References**

466

467 ACI (American Concrete Institute). 2019. *2019 Building Code Requirements for Structural*  
468 *Concrete*, ACI 318-19. Farmington Hills, MI: ACI

469

470 Adamcio, A. 2019. "Usable elements from wind turbine wings." Accessed November 21, 2019.

471 <https://www.anmet.com.pl/>

472

473 Agarwal, B.H., Broutman, L.J., and Chandrashekhara, K. 2006. *Analysis and Performance of*  
474 *Fiber Composites*, 3<sup>rd</sup> Edition, Pg. 549. Hoboken, NJ: John Wiley & Sons.

475

476 3A Core Materials. 2018. "AIREX<sup>®</sup> T92.200." Accessed November 21, 2019.

477 <https://www.3accorematerials.com/en/products/airex-foam/airex-t92-pet-foam>

478

479 Alshannaq, A., D. Scott, L. Bank, M. Bermek, and R. Gentry. 2019. "Structural re-use of de-  
480 commissioned wind turbine blades in civil engineering applications." In Proceedings of the  
481 American Society for Composites—Thirty-Fourth Technical Conference on Composite Material,  
482 DEStech Publications, Inc. 439 North Duke Street, Lancaster, Pennsylvania 17602-4967 USA,  
483 ISBN: 978-1-60595-602-2, USB flash drive or CD-ROM. <https://www.destechpub.com/>

484

485 Arias, F.R. 2016. "NuMAD Modeling and Finite Element Analysis of SNL-100-01 Wind  
486 Turbine Blade Shells." Independent Study Report, Department of Civil Engineering, City  
487 College of New York, NY. DOI: 10.13140/RG.2.2.18870.04161.

488

489 Arias, F.R. 2017. "Reusing composite materials from decommissioned wind turbine blades." MS  
490 Report, Department of Civil Engineering, City College of New York, NY. DOI:  
491 10.13140/RG.2.2.30509.23527

492

493 ASCE (American Society of Civil Engineers). 2016. *Minimum Design Loads and Associated*  
494 *Criteria for Buildings and Other Structures*. ASCE 7-16. Reston, VA, USA: ASCE

495

496 Bank, L.C. 2006. *Composites for Construction: Structural Design with FRP Materials*,

497 Hoboken, NJ: Wiley

498

499 Bank, L.C. and Gentry, T.R. 2001. "Development of a Pultruded Composite Material Highway

500 Guardrail," *Composites Part A: Applied Science and Manufacturing*, 32(9):1329-1338.

501 [https://doi.org/10.1016/S1359-835X\(01\)00086-0](https://doi.org/10.1016/S1359-835X(01)00086-0)

502

503 Bank, L.C., Arias, F.R., Yazdanbakhsh, A., Gentry, T.R., Al-Haddad, T., Chen, J.F. and

504 Morrow, R. 2018. "Concepts for Reusing Composite Materials from Decommissioned Wind

505 Turbine Blades in Affordable Housing." *Recycling*, 3(1), 3.

506 <https://doi.org/10.3390/recycling3010003>

507

508 Bank, L.C., Arias, F.R., Gentry, T.R., Al-Haddad, T., Tasistro-Hart, B. and Chen, J.F. 2019.

509 "Structural analysis of FRP parts from waste wind turbine blades for building reuse

510 applications," in *Advances in Engineering Materials, Structures and Systems: Innovations,*

511 *Mechanics and Applications*. Edited by A. Zingoni, 1520-1524. Boca Raton, FL: CRC Press.

512 ISBN 9781138386969.

513

514 Beauson, J., Madsen, B., Toncelli, C., Brøndsted, P., Ilsted Bech, J., 2016. "Recycling of

515 shredded composites from wind turbine blades in new thermoset polymer composites." *Compos.*

516 *Part A Appl. Sci. Manuf.* 90, 390–399. <https://doi.org/10.1016/j.compositesa.2016.07.009>

517



518 Berg, J.C. and Resor, B.R. 2012. *Numerical Manufacturing and Design Tool (NuMAD v2.0) for*  
519 *Wind Turbine Blades: User's Guide*. SAND2012-7028, Sandia National Laboratories,  
520 Albuquerque, NM.

521  
522 Bladesign. 2019. "Products." Accessed November 21, 2019. <https://www.bladesign.de/products>

523  
524 Borowicz, D.T. and Bank, L.C. 2013. "Effect of web reinforcement on the behavior of pultruded  
525 fiber-reinforced polymer beams subjected to concentrated loads." *Const and Bldg Mats*, 14, 347-  
526 357. <https://doi.org/10.1016/j.conbuildmat.2013.05.081>

527  
528 CEN (European Committee for Standardization). 1991. *Actions on structures. Eurocode 1*.  
529 Brussels, Belgium: CEN.

530  
531 CEN (European Committee for Standardization). 1992. *Design of concrete structures. Eurocode*  
532 *2*. Brussels, Belgium: CEN.

533  
534 DIRECTIVE 2008/98/EC. 2008. *DIRECTIVE 2008/98/EC OF THE EUROPEAN PARLIAMENT*  
535 *AND OF THE COUNCIL of 19 November 2008 on waste and repealing certain Directives*.  
536 22.11.2008 EN Official Journal of the European Union L 312/3.

537  
538 EUR (Publications Office of the European Union). 2016. *Prospect for new guidance in the*  
539 *design of FRP*. EUR 27666 EN. Accessed November 21, 2019.  
540 <http://publications.jrc.ec.europa.eu/repository/handle/JRC99714>

541

542

543 General Electric. 2019. "[Haliade-x offshore wind turbine platform](#)." Accessed November 21,

544 2019. <https://www.ge.com/renewableenergy/wind-energy/offshore-wind/haliade-x-offshore->

545 [turbine](#)

546

547 Griffith, T. 2013. *The SNL100-01 Blade: Carbon Design Studies for the Sandia 100-meter*

548 *Blade. SAND2013-1178*. Sandia National Laboratories, Albuquerque, NM, USA.

549

550 GWEC (Global Wind Energy Council). 2016. *Global Wind Energy Outlook – 2016*. Accessed

551 November 21, 2019. <http://gwec.net/publications/global-wind-energy-outlook/global-wind->

552 [energy-outlook-2016/](#)

553

554 ICC (International Code Council) 2018. *International Building Code*. Washington, DC: ICC.

555

556 Jensen, J.P. and Skelton, K. 2018. "Wind turbine blade recycling: experiences, challenges and

557 possibilities in a circular economy." *Ren. & Sust. Energy Reviews*. 97: 165-176.

558 <https://doi.org/10.1016/j.rser.2018.08.041>

559

560 Job, S., Leeke, G., Mativenga, P.T., Oliveux, G., Pickering, S. and Shuaib, N.A. 2016.

561 [Composites Recycling: Where are we now?](#) Accessed November 21. 2019.

562 <https://compositesuk.co.uk/system/files/documents/Recycling%20Report%202016.pdf>

563

564 Liu, P. and Barlow, C.Y. 2017. "Wind turbine blade waste in 2050." *Waste Management*, 62:  
565 229-240. <https://doi.org/10.1016/j.wasman.2017.02.007>

566

567 LS-DYNA. 2018. Version 4.5.21 May 2018. Livermore Software Technology Corporation,  
568 Livermore, CA. [www.lstc.com](http://www.lstc.com)

569

570 Mamanpush, S. H., Li, H., Englund, K., and Tabatabaei, A. T. (2018). Recycled wind turbine  
571 blades as a feedstock for second generation composites. *Waste Management*, 76, 708-714.

572 doi:10.1016/j.wasman.2018.02.050.

573

574 Mandell, J.F., D.D. Samborsky, D.D., 1997. *DOE / MSU Composite material fatigue database.*

575 *Version 19.0.* Sandia Technical Report, SAND97-3002. Sandia National Laboratories,

576 Albuquerque, NM, USA

577

578 Oliveux, G., Dandy, L., and Leeke, G. 2015. "Current status of recycling of fibre reinforced  
579 polymers: Review of technologies, reuse and resulting properties." *Prog. in Mat. Sci.* 72: 61-99.

580 <https://doi.org/10.1016/j.pmatsci.2015.01.004>

581

582 Post, N.L., Lesko, J.J., and Case, S.W., (2010), "Fatigue Life Prediction of Composites and  
583 Composite Structures", in *Fatigue Life Prediction of Composites and Composite Structures*,

584 Woodhead, pp. 79-101. <https://doi.org/10.1533/9781845699796.1.79>

585

- 586 Ramesh, N. Tasneem Abbasi, S. M. Tauseefand S.M., Abbasi, S.A. 2018. "Utilization of fiber-  
587 reinforced plastic (FRP) waste generated by a wind-turbine manufacturing company."  
588 *International Journal of Engineering & Scientific Research*, 6 (2) 103 – 129. Jagadhri, India  
589
- 590 Rhino3D. (2018). Rhinoceros V5.0 Educational. Robert McNeel & Associates, Seattle, USA.  
591 [www.rhino3d.com](http://www.rhino3d.com)  
592
- 593 Rodin, H., Somayeh Nassiri, R., Englund, K., Fakron, O., and Li, H., 2018. "Recycled glass fiber  
594 reinforced polymer composites incorporated in mortar for improved mechanical performance."  
595 *Const. and Build. Mats.* 187, 738-751. <https://doi.org/10.1016/j.conbuildmat.2018.07.169>  
596
- 597 Skelton, K. 2017. "Discussion paper on managing composite blade waste." WindEurope  
598 Technical Report. DOI: 10.13140/RG.2.2.22748.90248.  
599
- 600 Speksnijder, S., 2018. "Reuse of wind turbine blades in a slow traffic bridge." Accessed  
601 November 21, 2019. <http://www.stijnspeksnijder.com/gallery/bridge-of-blades/>  
602
- 603 SNL. 2019. *SNL/MSU/DOE 2019 Composite Material Database, Version 29*. Accessed  
604 November 21, 2019. [https://energy.sandia.gov/programs/renewable-energy/wind-power/blade-  
605 reliability/mhk-materials-database/](https://energy.sandia.gov/programs/renewable-energy/wind-power/blade-reliability/mhk-materials-database/)  
606
- 607 Suhail, R., Chen, J.-F., Gentry, R., Taristro-Hart, B., Xue, Y., Bank, L., 2019. "Analysis and  
608 Design of a Pedestrian Bridge with Decommissioned FRP Windblades and Concrete." In Proc.,

609 *14th Int. Symp. On Fiber-Reinforced Polymer Reinforcement of Concrete Structures*  
610 (FRPRCS14), Belfast, UK, Belfast, UK, June 4-7, 2019, paper no. 176. International Institute  
611 for FRP in Construction (IIFC), [https://www.iifc.org/publications/proceedings-iifc-official-](https://www.iifc.org/publications/proceedings-iifc-official-conferences/)  
612 [conferences/](https://www.iifc.org/publications/proceedings-iifc-official-conferences/)  
613  
614 SuperuseStudios, 2012. "REwind Willemsplein - Superuse Studios." Accessed November 21,  
615 2019. <https://www.superuse-studios.com/projects/rewind-willemsplein/>  
616  
617 Yazdanbakhsh, A., Bank, L.C., Rieder, K.A., Tian, Y., Chen, C., 2018. "Concrete with discrete  
618 slender elements from mechanically recycled wind turbine blades." *Resour. Conserv. Recycl.*  
619 128,11-21. <https://doi.org/10.1016/j.resconrec.2017.08.005>  
620

621 **List of Figures**

622

623

624 Fig. 1 Repurposing concepts for housing from 100 m long blade parts

625

626 Figure 2. a.) Entire 100-m long blade, b.) Cross-sectional view at Station 19 (27.6-m from the  
627 root end)

628

629 Fig. 3 Location of roof section extracted from blade (along the length)

630

631 Fig. 4 Schematic of roof

632

633 Fig. 5 Dimensions of the roof (perspective drawing)

634

635 Fig. 6 Analytical model of the shell panel and supports

636

637 Fig. 7 Analytical model of the shear web and supports

638

639 Fig. 8. FEM mesh and boundary conditions

640

641 Fig. 9. Z-displacement of the roof

642

643 Fig. 10. Stresses in top skin layer in  $y$ -direction (blade transverse or contour direction)

644

645 Fig. 11. Stresses in top skin layer in  $x$ -direction (blade longitudinal direction)

646

647 Fig. 12 Displacement of the shear webs in the  $Z$ -direction

648

649 Fig 13 Stresses in the shear webs in the  $x$ -direction (longitudinal direction of the web)

650

651 Fig 14 Stresses in the shear webs in the  $y$ -direction (vertical direction in the web)

652

653 Fig. 15 Buckled shape of the 3<sup>rd</sup> shear web

654

655

656

657 **List of Tables**

658

659

660 Table 1. Material properties of laminates in the SNL-100-01

661 Table 2. Hand-Calculation Overdesign Factors (ODFs) for Case 1 – Shell Panel

662 Table 3. Hand Calculation Overdesign Factors (ODFs) for Case 2 – Shear Web (T-Beam)

663 Table 4. 3-D FEM Calculation Overdesign Factors (ODFs) for entire roof

664

665 Figure 1.

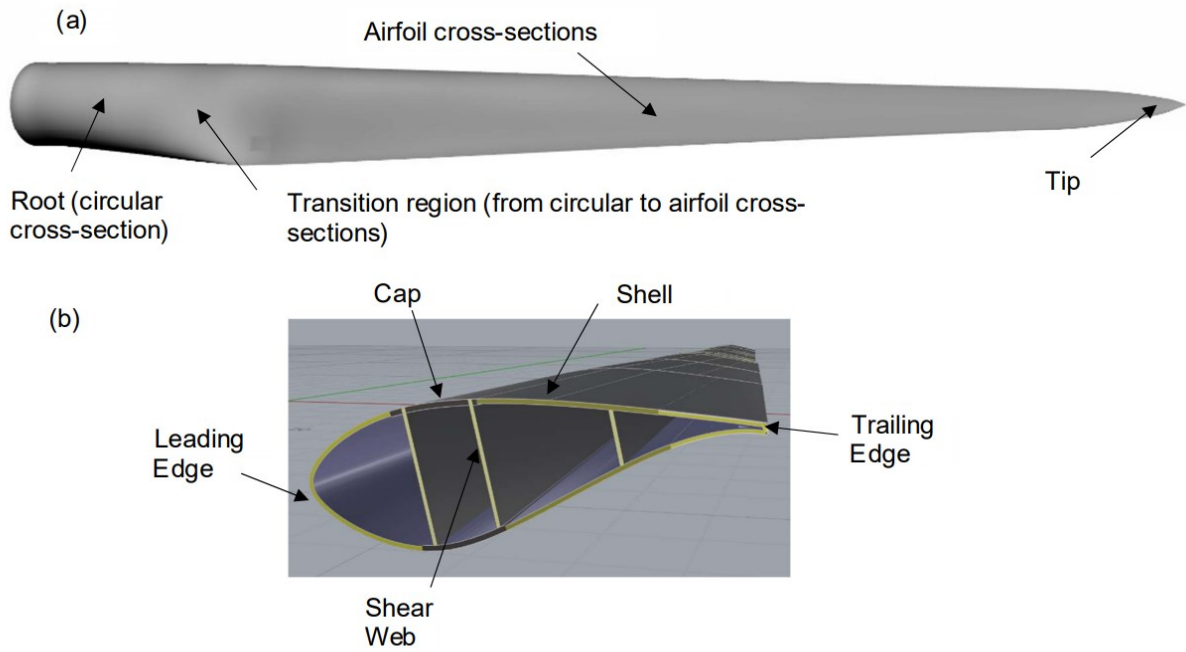


666

667



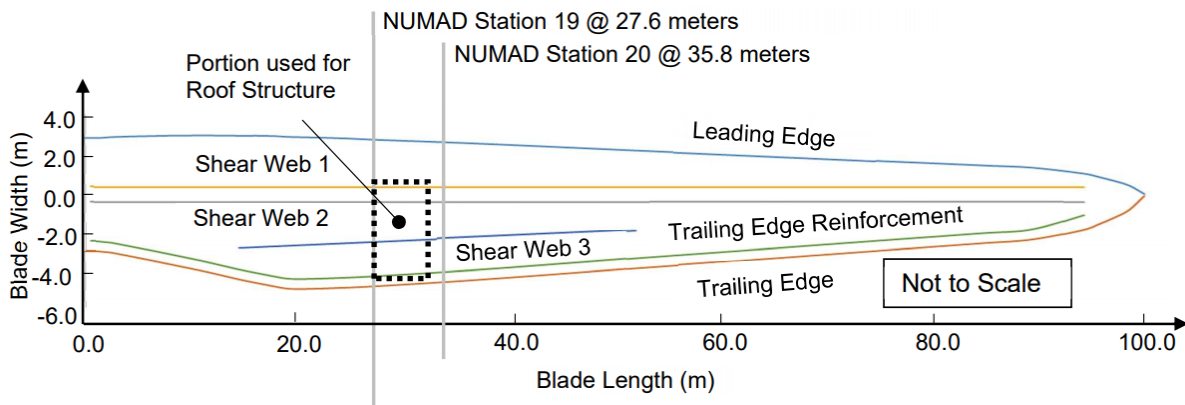
668 Figure 2



669

670

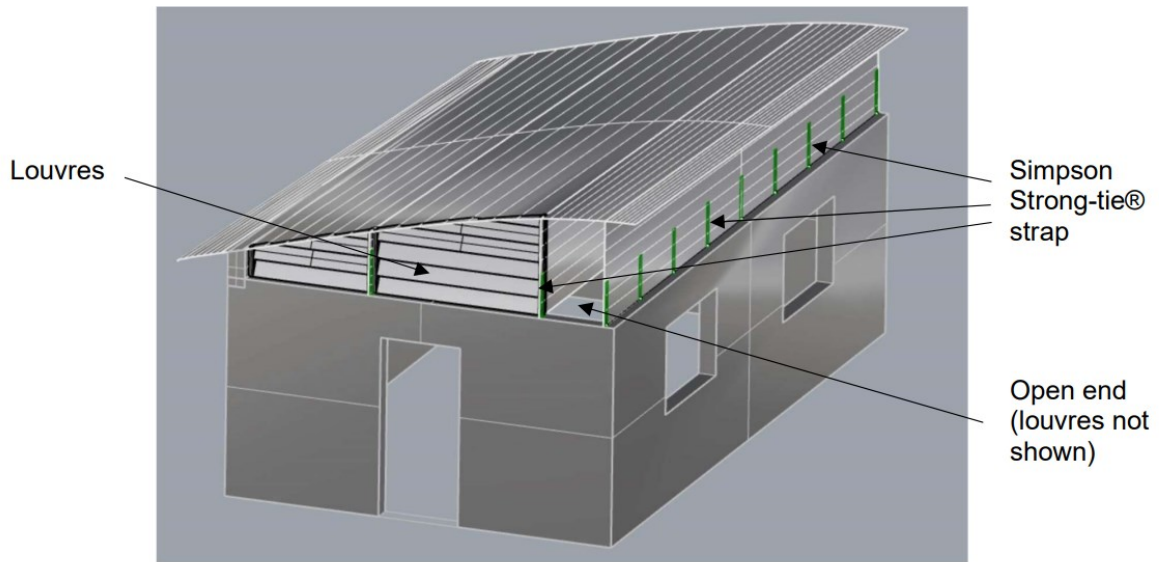
671 Figure 3



672

673

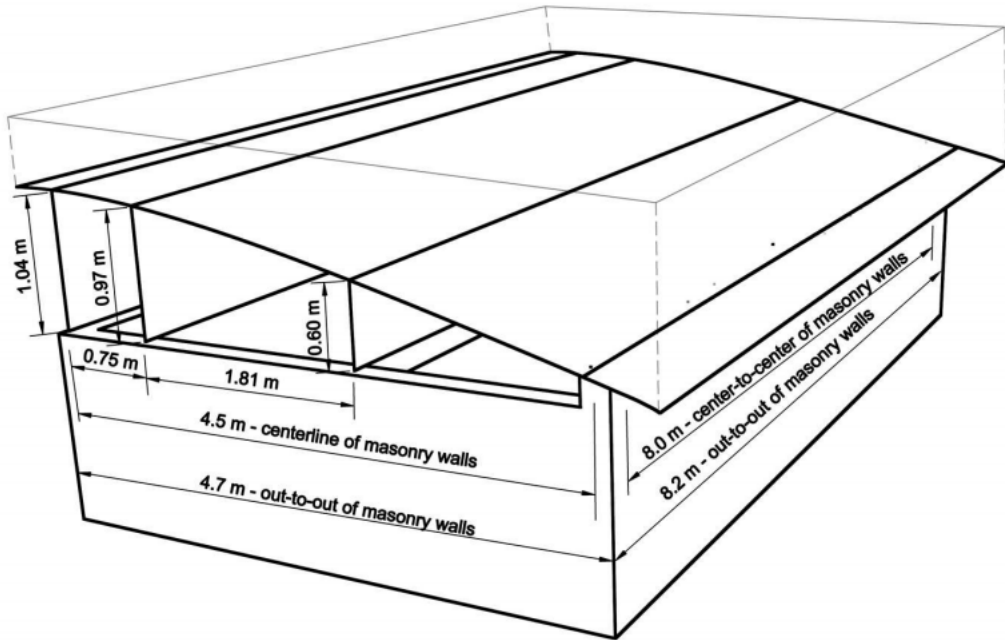
674 Figure 4



675

676

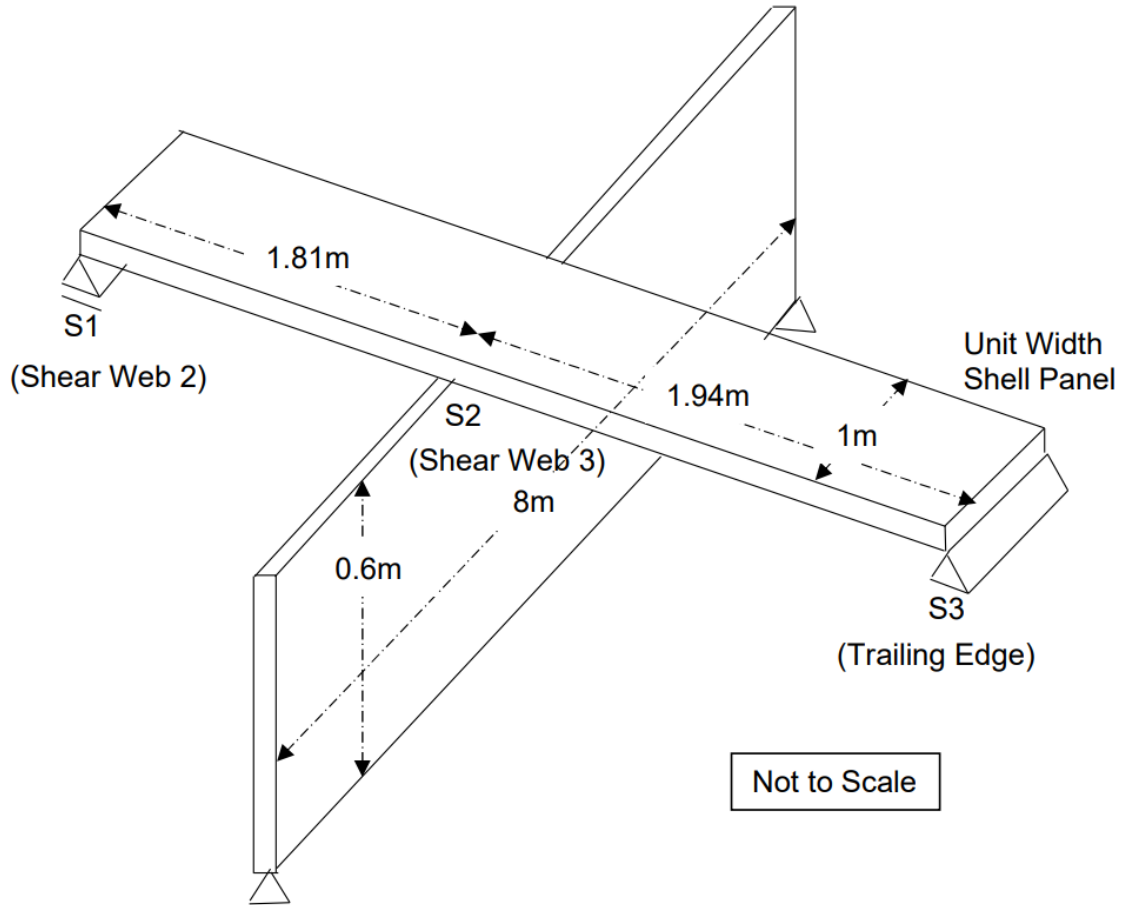
677 Figure 5



678

679

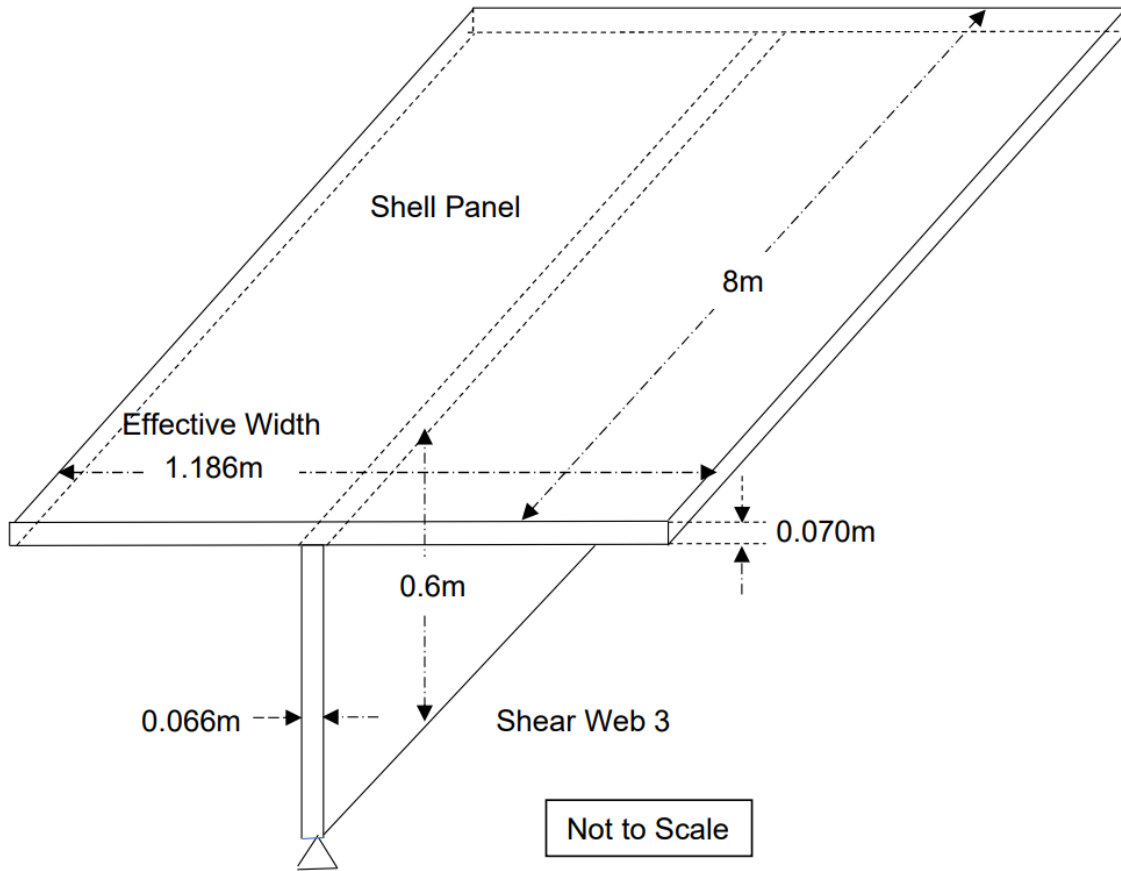
680 Figure 6



681

682

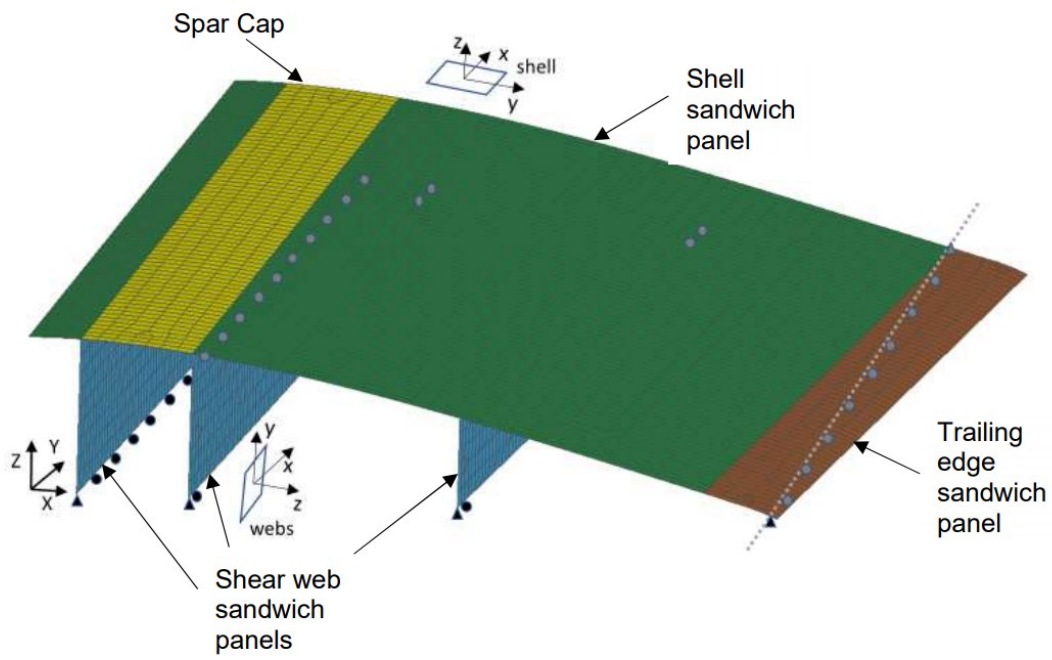
683 Figure 7



684

685

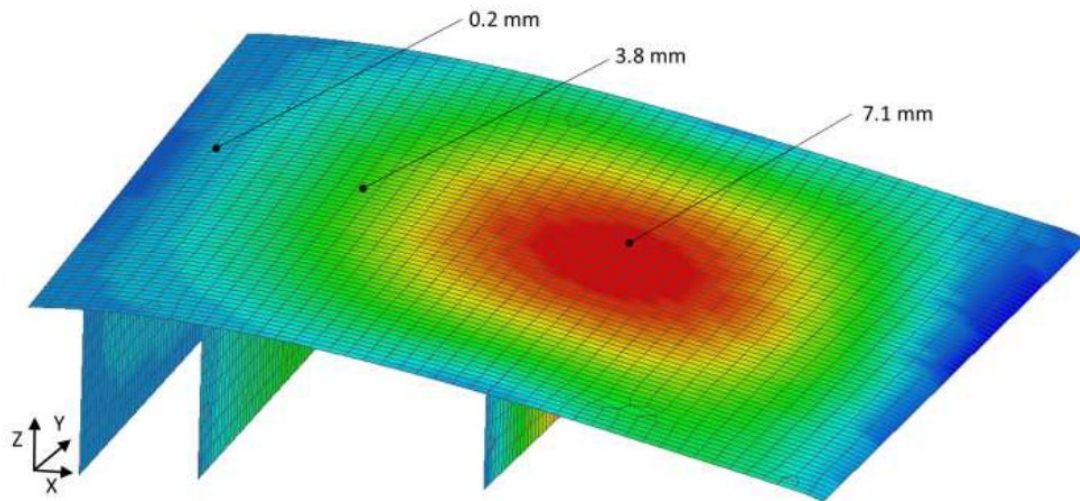
686 Figure 8



687

688

689 Figure 9

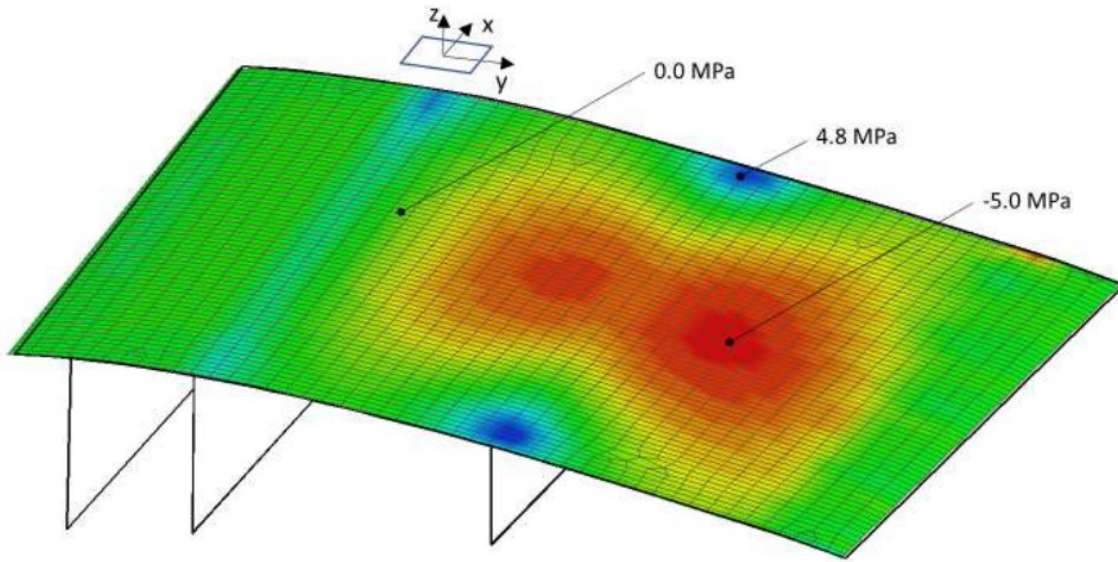


690

691



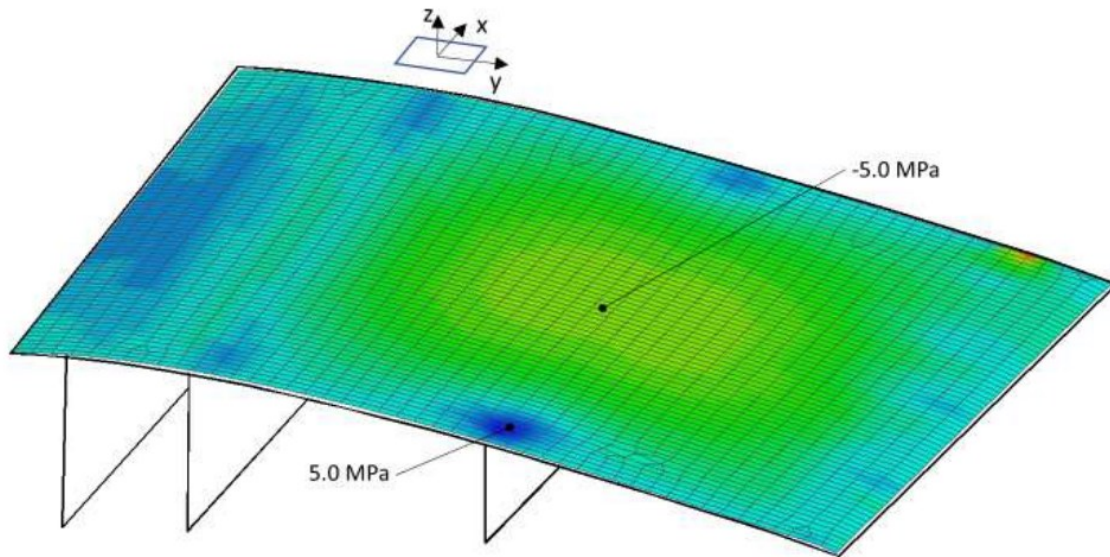
692 Figure 10



693

694

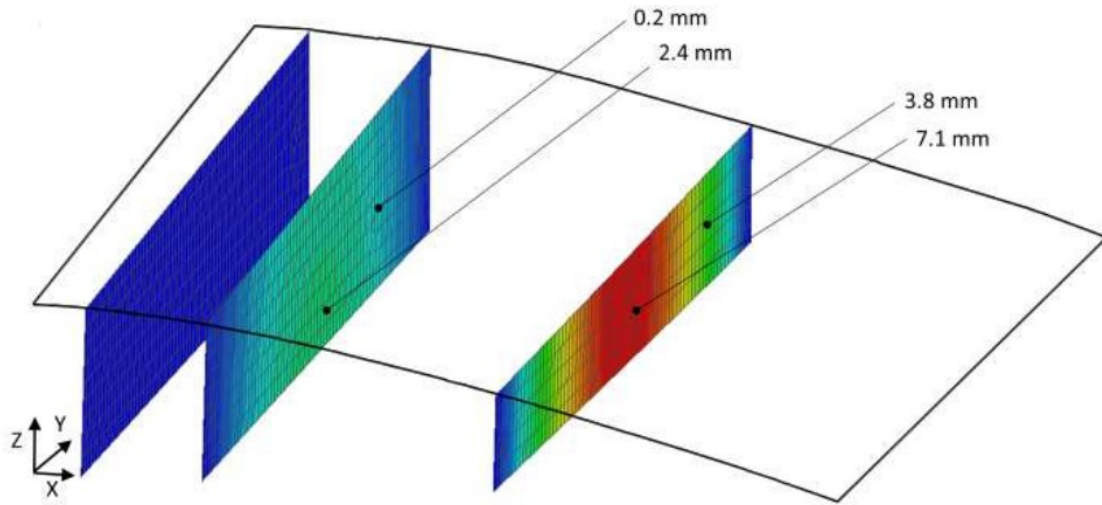
695 Figure 11



696

697

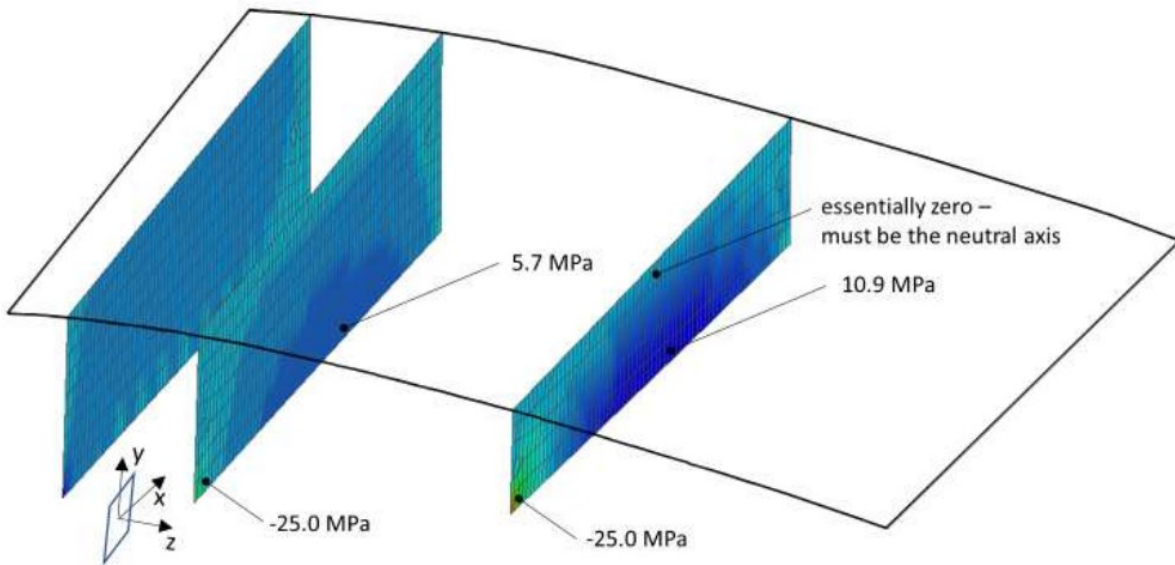
698 Figure 12



699

700

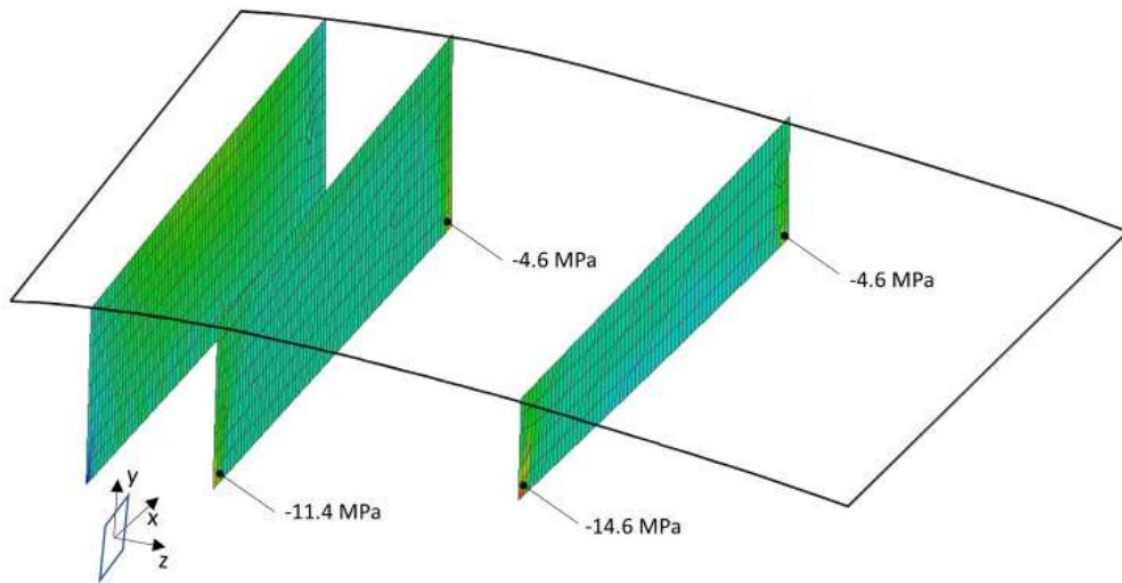
701 Figure 13



702

703

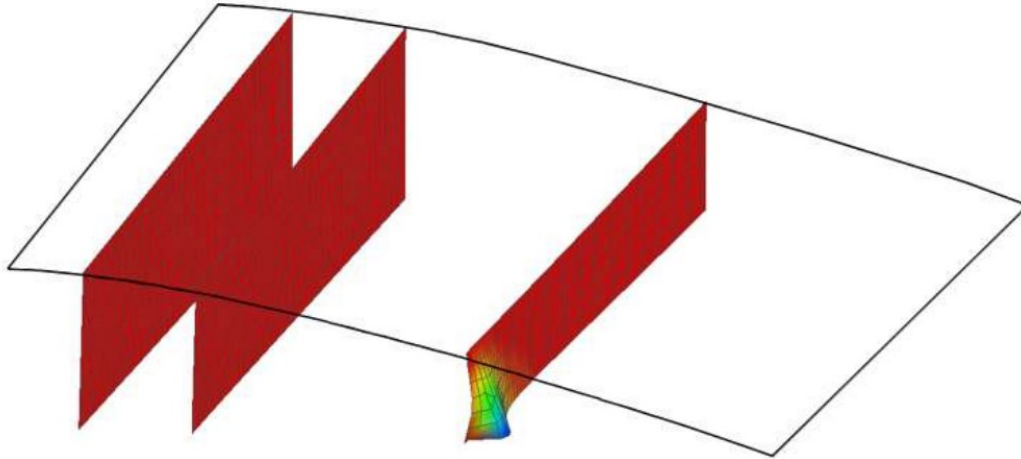
704 Figure 14



705

706

707 Figure 15



708

709

710  
711  
712  
713

Table 1. Material properties of laminates in the SNL-100-01

714  
715  
716  
717  
718  
719  
720  
721  
722  
723  
724  
725  
726  
727  
728  
729  
730  
731  
732  
733  
734  
735  
736  
737  
738  
739  
740  
741

Material Type	$E_{11}$ (GPa)	$E_{22}$ (GPa)	$G_{12}$ (GPa)	$\nu_{12}$	$\rho$ (kg/m <sup>3</sup> )	$\sigma_{11}$ (tens) (MPa)	$\sigma_{11}$ (comp) (MPa)	$\sigma_{22}$ (tens) (MPa)	$\sigma_{22}$ (comp) (MPa)	$\tau$ (MPa)
Foam	0.256	0.256	0.022	0.3	200	3.1 <sup>#</sup>	-3.8 <sup>#</sup>	3.1 <sup>#</sup>	-3.8 <sup>#</sup>	2.0 <sup>#</sup>
Glass UD [0] <sub>2</sub>	41.80	14.00	2.63	0.28	1920	972	-702	31 <sup>*</sup>	-118 <sup>*</sup>	72 <sup>*</sup>
SNLBiax [±45] <sub>4</sub>	13.60	13.30	11.80	0.51	1780	144	-213	144	-213	--
SNLTriax [±45] <sub>4</sub> [0] <sub>2</sub>	27.70	13.65	7.20	0.39	1850	972	-702	144 <sup>§</sup>	-213 <sup>§</sup>	--
SNLCarbon (UD)	114.50	8.39	5.99	0.27	1220	1546	-1047	52 <sup>*</sup>	-206 <sup>*</sup>	93 <sup>*</sup>
Notes: # from AIREX <sup>®</sup> T92.200 (2018) * from Agarwal et al (2006) § assumes that ±45plies control strength in transverse direction -- not determined (not used in analysis)										

742

Table 2. Hand-Calculation Overdesign Factors (ODFs) for Case 1 – Shell Panel

Stress or Displacement Component Analyzed	Hand-Calculated Value (MPa or mm)	Relevant Design Property	Ultimate Value (MPa or mm)	Partial Safety Factor ( $\gamma_M$ )	Code Allowable (MPa or mm)	ODF = Allowable/Calculated Values
$\sigma_{\text{Triax\_top}}$	+5.26	$\sigma_{22\text{tens(Triax)}}$	+144	1.86	+77.4	14.7
$\sigma_{\text{Triax\_bottom}}$	-5.26	$\sigma_{22\text{comp(Triax)}}$	-213	1.86	-114.5	21.7
$\sigma_{\text{foam}}$	+0.085	$\sigma_{\text{tens(foam)}}$	+3.1	1.86	+1.7	19.6
$\sigma_{\text{foam}}$	-0.085	$\sigma_{\text{comp(foam)}}$	-3.8	1.86	-2.0	24.0
$\tau_{\text{foam}}$	+0.045	$\tau_{\text{ult(foam)}}$	+2.0	1.86	+1.1	23.9
$\delta_{\text{midspan}}$	12.08	L(3650)/240	15.6	1.0	15.6	1.29

743

744



745  
746  
747

Table 3. Hand Calculation Overdesign Factors (ODFs) for Case 2 – Shear Web (T-Beam)

748

Stress or Displacement Component Analyzed	Hand-Calculated Value (MPa or mm)	Relevant Design Property	Ultimate Value (MPa or mm)	Partial Safety Factor ( $\gamma_M$ )	Code Allowable (MPa or mm)	ODF = Allowable/Calculated Values
$\sigma_{\text{Triax\_top}}$	-10.06	$\sigma_{11\text{comp(Triax)}}$	-702	1.86	-377.4	37.5
$\sigma_{\text{Biax\_skin}}$	+36.06	$\sigma_{11\text{tens(Biax)}}$	+144	1.86	+77.4	2.1
$\sigma_{\text{foam\_shell}}$	-0.087	$\sigma_{\text{comp(foam)}}$	-3.8	1.86	-2.0	23.0
$\sigma_{\text{foam\_web}}$	-0.680	$\sigma_{\text{comp(foam)}}$	-3.8	1.86	-2.0	2.9
$\tau_{\text{foam\_web}}$	+0.462	$\tau_{\text{ult(foam)}}$	+2.0	1.86	+1.1	2.4
$\delta_{\text{midspan}}$	29.9	L(8000)/240	33.3	1.0	33.3	1.1

749  
750

751

Table 4. 3-D FEM Calculation Overdesign Factors (ODFs) for entire roof

752

Stress or Displacement Component Analyzed	Hand-Calculated Value (MPa or mm)	Relevant Design Property	Ultimate Value (MPa or mm)	Partial Safety Factor ( $\gamma_M$ )	Code Allowable (MPa or mm)	ODF = Allowable/Calculated Values
$\sigma_{yTriax\_top}$	-5.0	$\sigma_{11comp}(Triax)$	-702	1.86	-377.4	75.5
$\sigma_{yTriax\_top}$	+4.8	$\sigma_{11tens}(Triax)$	+972	1.86	+552.6	108.9
$\sigma_{xTriax\_top}$	-5.0	$\sigma_{22comp}(Triax)$	-213	1.86	-114.5	22.9
$\sigma_{xTriax\_top}$	+5.0	$\sigma_{22tens}(Triax)$	+144	1.86	+77.4	15.5
$\sigma_{xBiax\_bottom}$	+10.9	$\sigma_{11tens}(Biax)$	+144	1.86	+77.4	7.3
$\sigma_{xBiax\_bottom}$	-25.0	$\sigma_{11comp}(Biax)$	-213	1.86	-114.5	4.6
$\sigma_{yBiax\_bottom}$	-14.6	$\sigma_{22comp}(Biax)$	-213	1.86	-114.5	7.8
$\delta_{shell}$	7.1	3750/240	15.6	1.0	15.6	2.2
$\delta_{web}$	7.1	8000/240	33.3	1.0	33.3	4.7

753